Supplementary Material of "Anisotropic Total Variation Regularized Tensor Ring Decomposition for OCT Images Denoising and Super-resolution"

Parisa Ghaderi Daneshmand[1], Hossein Rabbani[*,1], Senior Member, IEEE

[1]Medical Image & Signal Processing Research Center, School of Advanced Technologies in Medicine, Isfahan University of Medical Sciences, Isfahan, Iran

I. Overview

This supplementary material includes the following sections. Section II presents more visual results for the noise suppression experiment of dataset-1. In Section III, we provided the quantitative and qualitative results for denoising OCT images of dataset-3. Section IV presents more visual results for super-resolution of OCT images of dataset-1 with 50% missing rate. In Section V, we provided visual results for super-resolution of OCT images of dataset-1 with 75% missing rate. Section VI presents an ablation study in the OCT denoising experiment using the dataset-1. Finally, we validated the robustness of our proposed TRFOTTV model for different speckle noise levels in Section VII.

[*]Corresponding author

II. OCT Images Denoising Results for Dataset-1

This section provides more visual results for the noise suppression experiment of dataset-1.Fig.S1 presents a visual comparison between the proposed TRFOTTV method and rival methods for the denoising of one retinal OCT image in dataset-1.

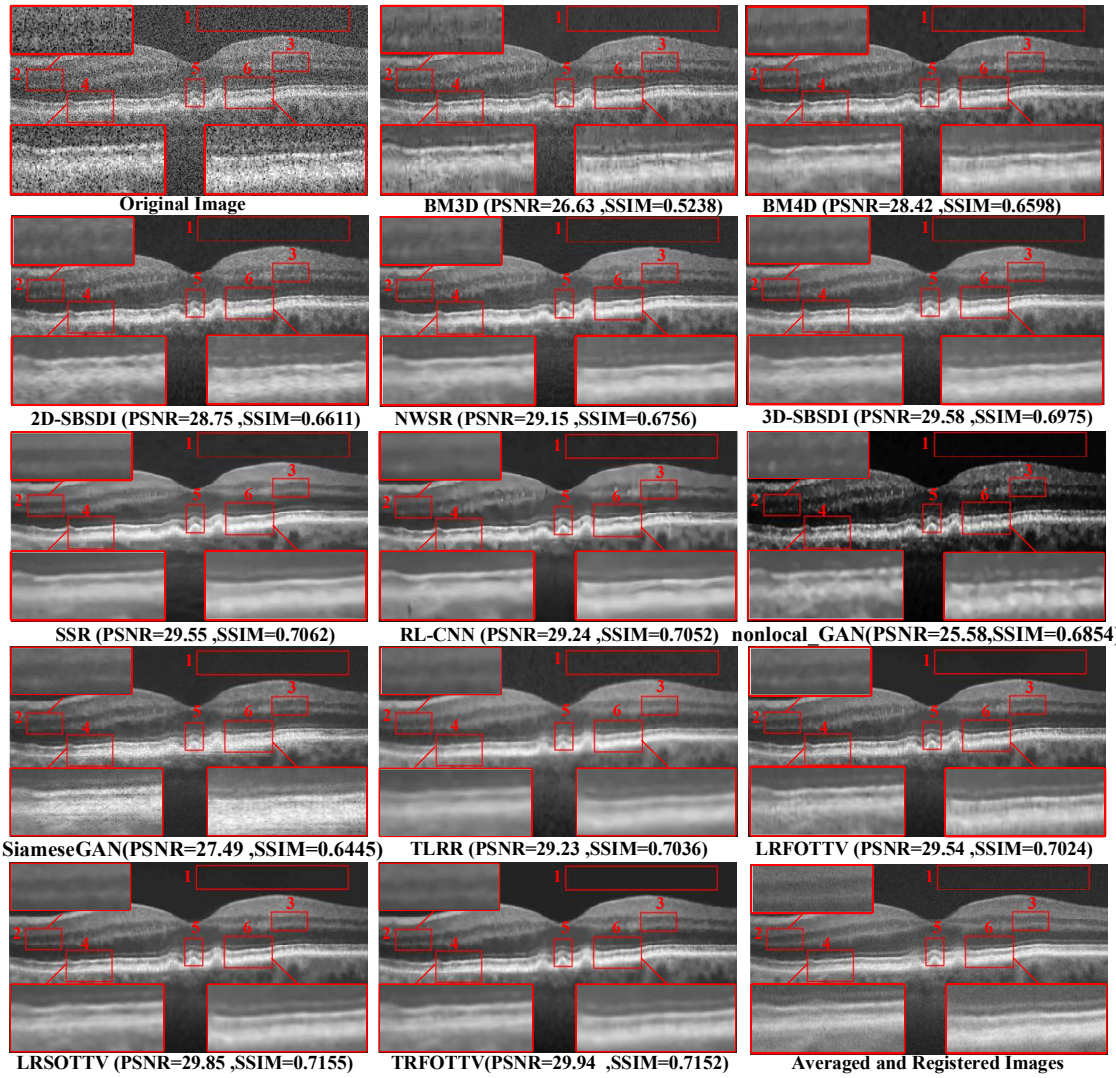

Fig.S1 One retinal OCT image in the dataset-1 and their denoising results utilizing the BM3D [1], BM4D [2], 2D-SBSDI [3], NWSR [4], 3D-SBSDI [3], SSR [5], RL-CNN [6], nonlocal_GAN [7], SiameseGAN [8], TLRR [9], LRFOTTV [10], LRSOTTV [10], and the suggested approach.

III. Results for OCT Images Denoising of Dataset-3

This section provides qualitative and quantitative results for the noise suppression experiment of dataset-3. Fig.S2 and Table. S1 show results of all compared techniques. As Fig.S2 shows, the proposed TRFOTTV has the most pleasing performance in maintaining layer structures and reducing the noise. Moreover, this method outperforms other rival methods in terms of CNR, and MSR.

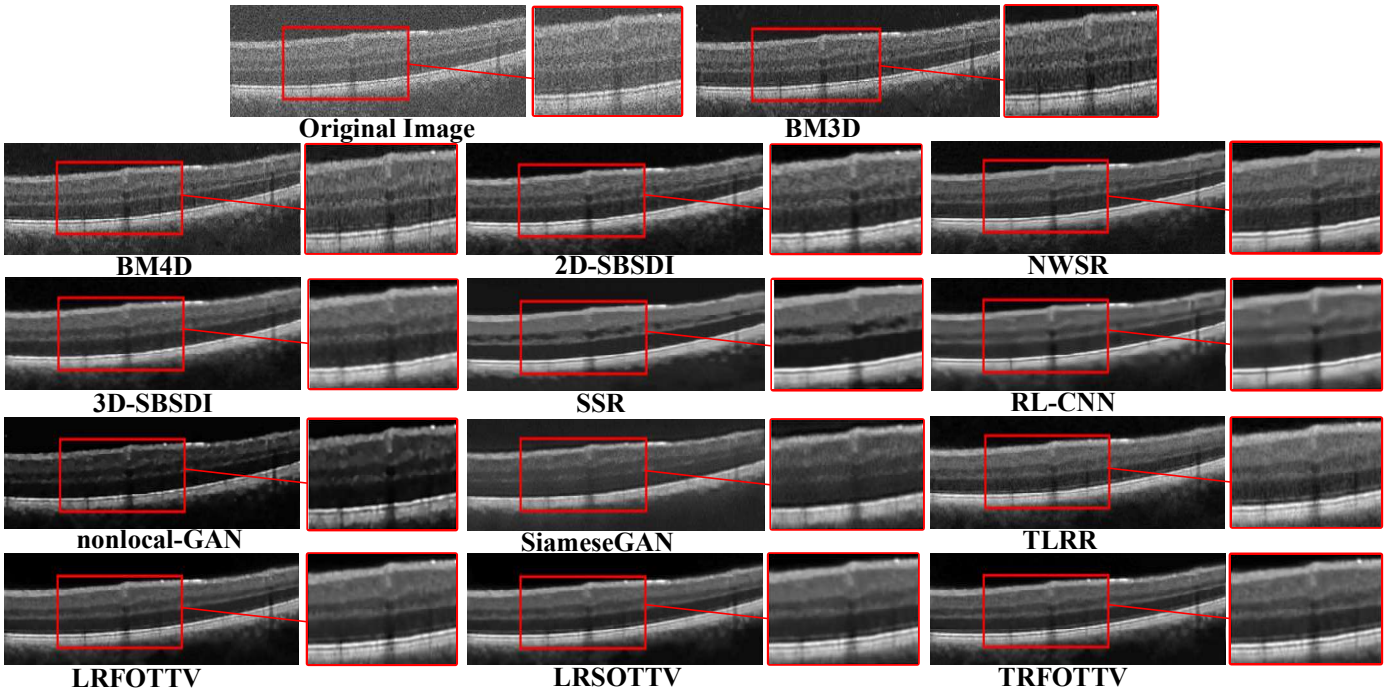

Fig.S2 One retinal OCT image in the dataset-3 and their denoising results utilizing the BM3D [1], BM4D [2], 2D-SBSDI [3], NWSR [4], 3D-SBSDI [3], SSR [5], RL-CNN [6], nonlocal_GAN [7], SiameseGAN [8], TLRR [9], LRFOTTV [10], LRSOTTV [10], and the suggested approach.

Table.S1 Mean & Standard deviation of the MSR and CNR results for denoising the dataset-3 by various approaches. Best results are bolded. Where $p < 0.05$, the measures for each test approach are statistically meaningful and characterized by a* symbol.

	CNR		MSR	
	Mean± SD	P-value	Mean± SD	P-value
BM3D	3.09±0.86	1.96E-04*	5.92±1.50	1.96E-04*
BM4D	3.48±1.15	1.96E-04*	7.24±2.36	1.96E-04*
2D-SBSDI	4.15±1.69	7.38E-04*	9.12±3.67	4.55E-04*
NWSR	4.07±1.74	3.27E-04*	9.32±4.00	1.96E-04*
3D-SBSDI	4.51±2.01	1.59E-03*	11.14±5.16	5.36E-04*
SSR	4.18±2.11	1.17E-03*	11.08±6.24	2.47E-03*
RL-CNN	4.46±2.04	7.39E-03*	4.83±2.30	1.96E-04*
nonlocal-GAN	2.78±1.13	1.96E-04*	11.61±5.34	1.76E-02*
SiameseGAN	3.69±1.52	1.96E-04*	10.93±5.46	1.84E-03*
TLRR	4.39±1.78	5.68E-03*	10.35±4.29	1.17E-03*
LRFOTTV	4.42±1.81	3.27E-04*	11.58±5.61	1.96E-04*
LRSOTTV	4.59±1.95	3.77E-03*	12.33±5.97	3.46E-02*
TRFOTTV	**4.66±2.03**	-	**13.09±6.67**	-

IV. Results for OCT Images Super-Resolution of Dataset-1 with 50% missing rate

This section presents more visual results for super-resolution of OCT images of dataset-1 with 50% missing rate. Fig.S3 shows a visual comparison between the proposed TRFOTTV method and compared methods for super-resolution of OCT images with 50% data missing on synthetic subsampled images of dataset-1.

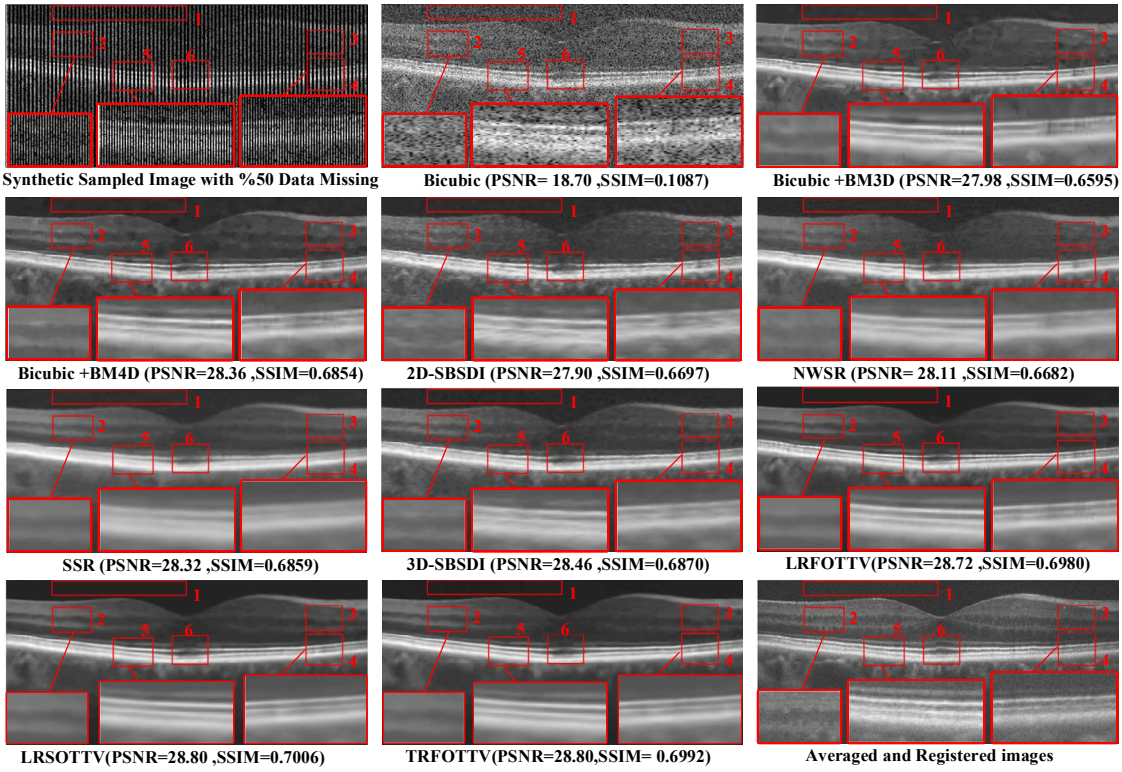

Fig.S3 One synthetic subsampled image in the first dataset (with 50% data missing) and the super-resolution results by utilizing the bicubic, BM3D [1] + bicubic, BM4D [2] + bicubic, 2D-SBSDI [3], NWSR [4], 3D-SBSDI [3], SSR [5], LRFOTTV [10], LRSOTTV [10], and the suggested approach.

V. Results for OCT Images Super-Resolution of Dataset-1 with 75% missing rate

This part presents visual results for super-resolution of OCT images of dataset-1 with 75% missing rate. Fig.S4 and Fig.S5 represent a visual comparison between the proposed TRFOTTV method and rival methods for super-resolution of OCT images with 75% data missing on synthetic subsampled images of dataset-1.

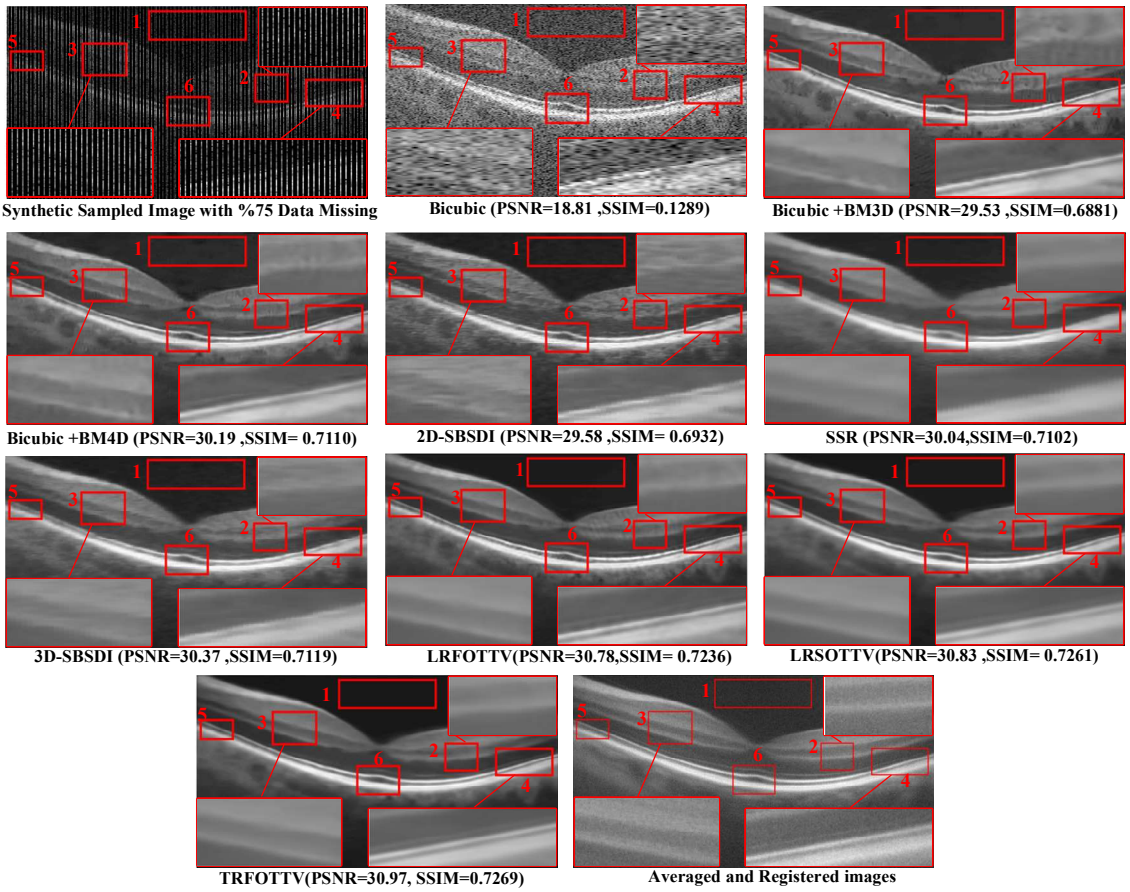

Fig.S4 One synthetic subsampled image in the first dataset (with 75% data missing) and the super-resolution results by utilizing the bicubic, BM3D [1] + bicubic, BM4D [2] + bicubic, 2D-SBSDI [3], 3D-SBSDI [3], SSR [5], LRFOTTV [10], LRSOTTV [10], and the suggested approach.

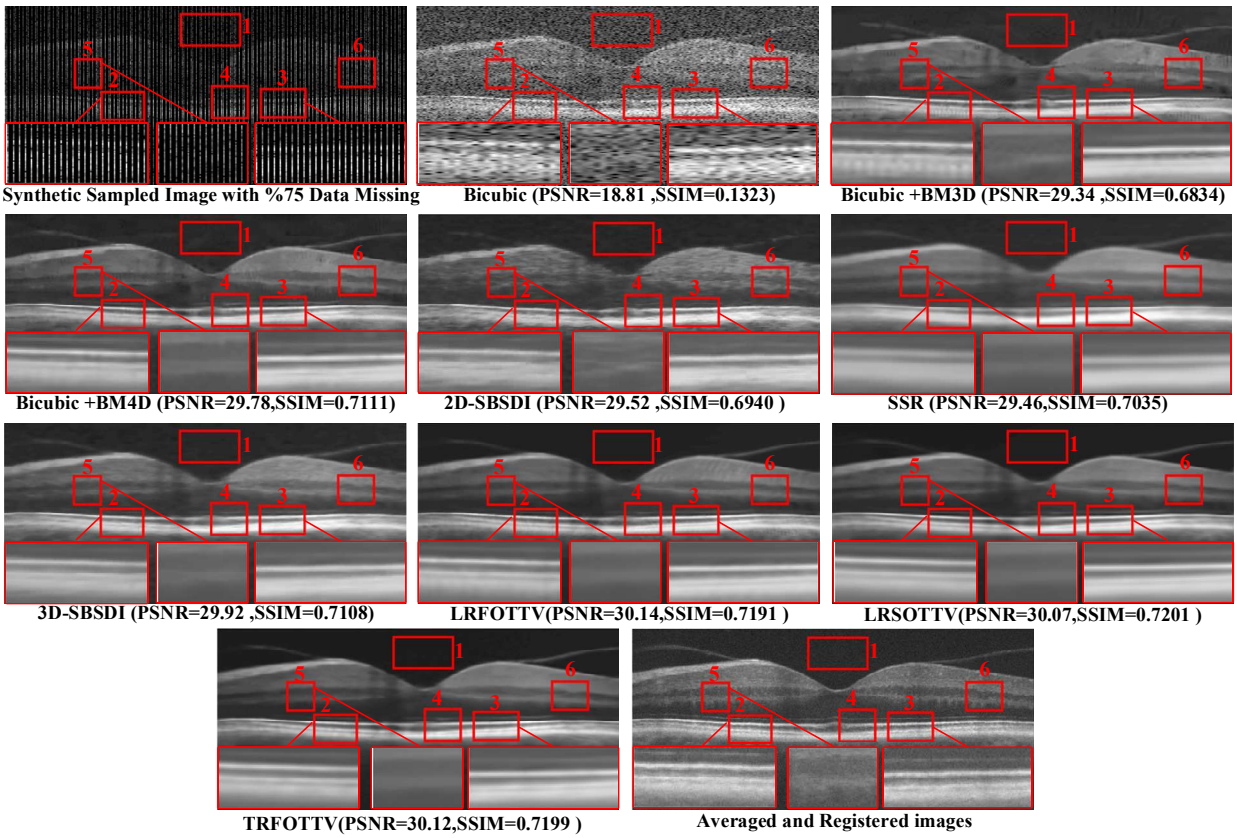

Fig.S5 One synthetic subsampled image in the first dataset (with 75% data missing) and the super-resolution results by utilizing the bicubic, BM3D [1] + bicubic, BM4D [2] + bicubic, 2D-SBSDI [3], 3D-SBSDI [3], SSR [5], LRFOTTV [10], LRSOTTV [10], and the suggested approach.

VI. Ablation Study

To further analyze the contribution of each model, we conducted an ablation study in the OCT denoising experiment using the dataset-1. Table.S2 demonstrates the results of this study. The last row of Table corresponds to the denoising results of the suggested TRFOTTV model (like as results of Table 1 in the manuscript). As Table S2 shows, using just smoothness prior via the FOTTV model cannot satisfactorily decrease the severe noise of OCT images. Moreover, the results of the TR model show that this model provides better performance in noise suppression by capturing the spatial, non-local, and temporal correlation priors of the OCT tensor data. The benefit of simultaneous use of all priors can obviously be seen by noticing that the TRFOTTV model significantly enhances the quantitative results in terms of SSIM, CNR, MSR, and PSNR.

Table.S2 Results of the ablation study for denoising the dataset-1.

		CNR	MSR	PSNR	SSIM
FOTTV	**Mean**	4.07	10.57	22.08	0.6010
	SD	1.23	2.38	1.55	0.0309
TR	**Mean**	4.47	16.93	28.04	0.6848
	SD	1.55	7.43	2.72	0.0354
TRFOTTV	**Mean**	**4.83**	**19.25**	**28.50**	**0.6977**
	SD	1.63	8.45	2.70	0.0307

VII. Robustness on TRFOTTV method for Different speckle Noise Levels

In this section, we validated the robustness of our proposed TRFOTTV method for different speckle noise levels. For this purpose, given that the proposed TRFOTTV method is a three-dimensional model, we require at least three B-scans as the input of our algorithm. Therefore, to evaluate the performance of our TRFOTTV model in reducing speck noise, we must have a clean OCT volume of at least three B-scans and artificially add speckle noise to it. Due to the fact that the dataset-1 for each subject consists of 5 noisy B-scans and only one clean B-scan (a high SNR-high-resolution (HH) image) and we do not have access to clean OCT volume, to generate clean 3D OCT volumes, we used the LRSOTTV method [10] which is one of the state-of-the-art OCT denoising techniques that have been proposed recently. Then, using this method, we generated clean 3D OCT volumes in the dataset-1. Next, we artificially added speckle noise with various strengths to the clean 3D OCT volumes and validated the robustness of our proposed TRFOTTV model for different speckle noise levels. For this purpose, the speckle noise model is formulated as:

$$\mathcal{Y} = \mathcal{X} + \mathcal{X}.\mathcal{V} \qquad \text{(S.1)}$$

where $\mathcal{X}$ represents the clean OCT tensor and $\mathcal{V} \sim N(0, \sigma^2)$ denotes multiplicative noise part. In our experiment, we considered for σ^2 (or noise variance) ranges from 0.02 to 0.2. Fig.S6 and Fig.S7 present the denoising result of the OCT images artificially corrupted by speckle noise with different noise values for two sample subjects in dataset-1.

As can be observed in Fig.S6 and Fig.S7, our proposed TRFOTTV method is strong technique for speckle noise suppression in OCT images and can preserve the layer structural details in these images. Moreover, for various speckle noise levels, TRFOTTV method efficiently removes the noise to differing degrees. When the speckle noise level increases, the performance of TRFOTTV method decays slightly. In summary, the proposed TRFOTTV method is robust to various speckle noise levels to a large extent.

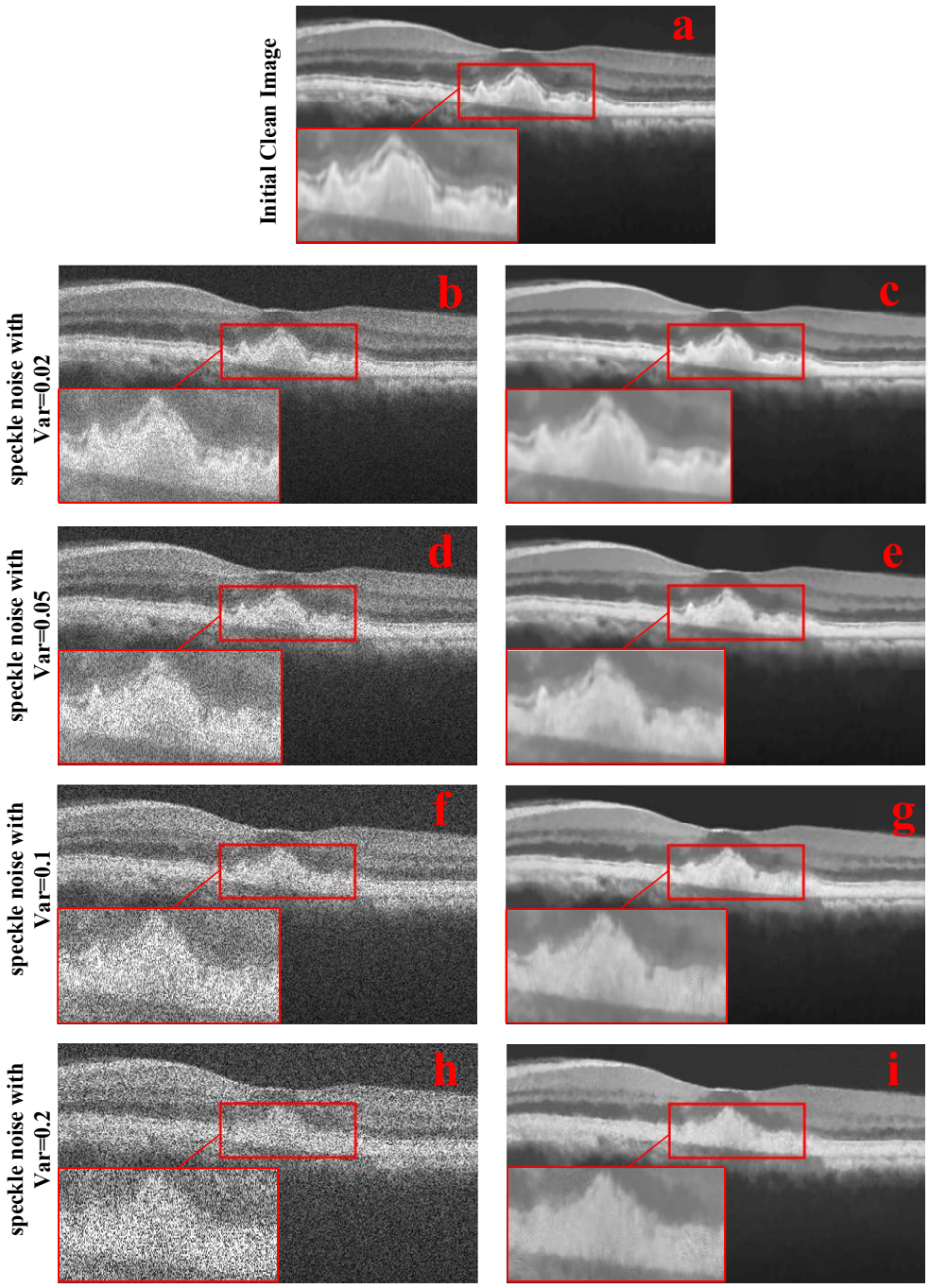

Fig.S6 Visual results for denoising result of the OCT images artificially corrupted by speckle noise with different variance (or σ^2values). (a) Clean OCT image (b-c) OCT image corrupted by speckle noise with Var=0.02, and the corresponding denoised image by TRFOTTV model. (d-e) OCT image corrupted by speckle noise with Var=0.05, and the corresponding denoised image by TRFOTTV model. (f-g) OCT image corrupted by speckle noise with Var=0.1, and the corresponding denoised image by TRFOTTV model. (h-i) OCT image corrupted by speckle noise with Var=0.2, and the corresponding denoised image by TRFOTTV model.

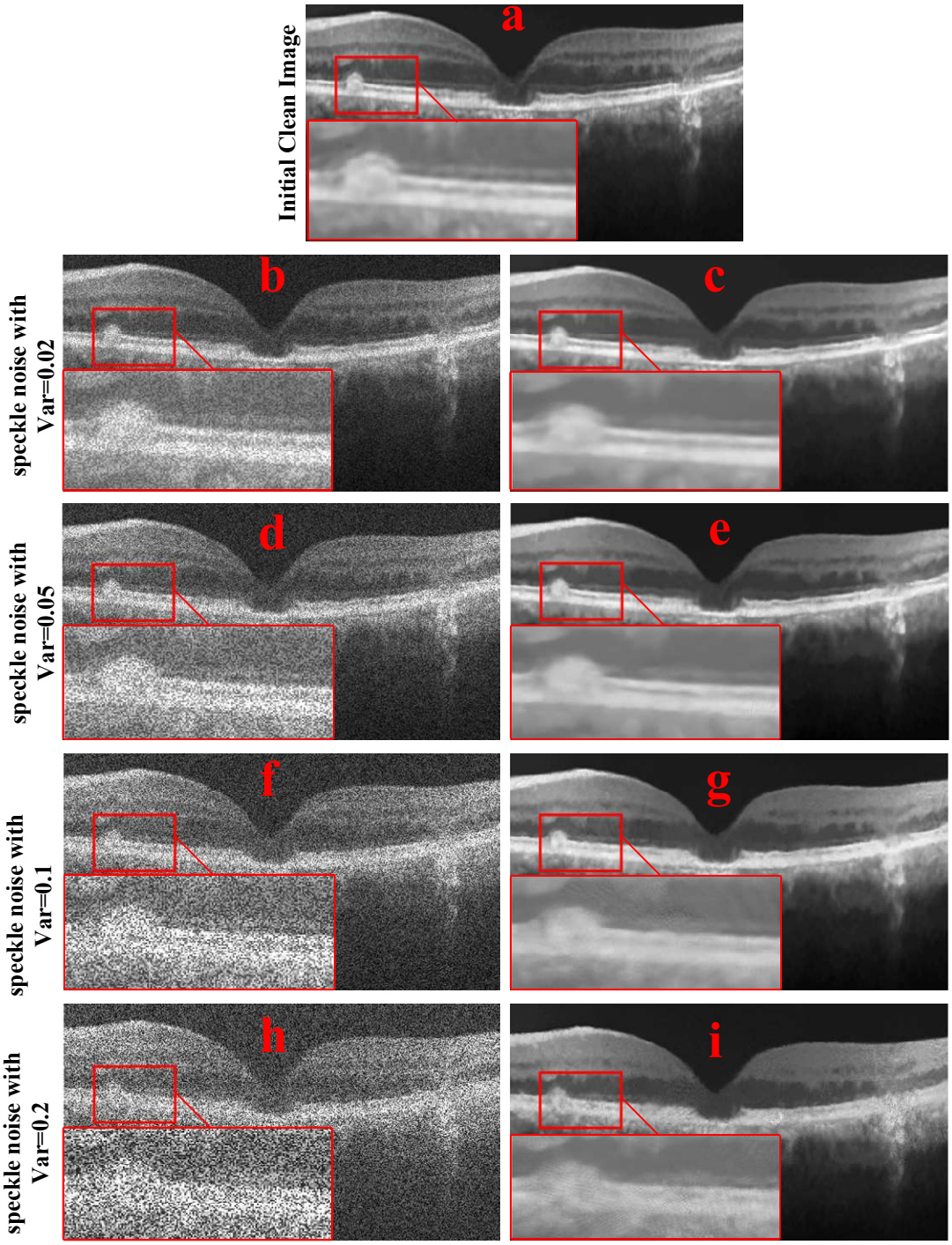

Fig.S7 Visual results for denoising result of the OCT images artificially corrupted by speckle noise with different variance (or σ^2values). (a) Clean OCT image (b-c) OCT image corrupted by speckle noise with Var=0.02, and the corresponding denoised image by TRFOTTV model. (d-e) OCT image corrupted by speckle noise with Var=0.05, and the corresponding denoised image by TRFOTTV model. (f-g) OCT image corrupted by speckle noise with Var=0.1, and the corresponding denoised image by TRFOTTV model. (h-i) OCT image corrupted by speckle noise with Var=0.2, and the corresponding denoised image by TRFOTTV model.

Bibliography

[1] K. Dabov, A. Foi, V. Katkovnik, and K. Egiazarian, "Image denoising by sparse 3-D transform-domain collaborative filtering," *IEEE Transactions on image processing,* vol. 16, no. 8, pp. 2080-2095, 2007.

[2] M. Maggioni, V. Katkovnik, K. Egiazarian, and A. Foi, "Nonlocal transform-domain filter for volumetric data denoising and reconstruction," *IEEE transactions on image processing,* vol. 22, no. 1, pp. 119-133, 2012.

[3] L. Fang *et al.*, "Fast acquisition and reconstruction of optical coherence tomography images via sparse representation," *IEEE transactions on medical imaging,* vol. 32, no. 11, pp. 2034-2049, 2013.

[4] A. Abbasi, A. Monadjemi, L. Fang, and H. Rabbani, "Optical coherence tomography retinal image reconstruction via nonlocal weighted sparse representation," *Journal of biomedical optics,* vol. 23, no. 3, p. 036011, 2018.

[5] L. Fang, S. Li, D. Cunefare, and S. Farsiu, "Segmentation based sparse reconstruction of optical coherence tomography images," *IEEE transactions on medical imaging,* vol. 36, no. 2, pp. 407-421, 2016.

[6] N. Gour and P. Khanna, "Speckle denoising in optical coherence tomography images using residual deep convolutional neural network," *Multimedia Tools and Applications,* vol. 79, no. 21, pp. 15679-15695, 2020.

[7] A. Guo, L. Fang, M. Qi, and S. Li, "Unsupervised denoising of optical coherence tomography images with nonlocal-generative adversarial network," *IEEE Transactions on Instrumentation and Measurement,* vol. 70, pp. 1-12, 2020.

[8] N. A. Kande, R. Dakhane, A. Dukkipati, and P. K. Yalavarthy, "SiameseGAN: a generative model for denoising of spectral domain optical coherence tomography images," *IEEE Transactions on Medical Imaging,* vol. 40, no. 1, pp. 180-192, 2020.

[9] P. Zhou, C. Lu, J. Feng, Z. Lin, and S. Yan, "Tensor low-rank representation for data recovery and clustering," *IEEE transactions on pattern analysis and machine intelligence,* vol. 43, no. 5, pp. 1718-1732, 2019.

[10] P. G. Daneshmand, A. Mehridehnavi, and H. Rabbani, "Reconstruction of optical coherence tomography images using mixed low rank approximation and second order tensor based total variation method," *IEEE Transactions on Medical Imaging,* vol. 40, no. 3, pp. 865-878, 2020.